Palynological evidence for the Mid-Miocene Climatic Optimum recorded in Cenozoic sediments of the Tian Shan Range, northwestern China

Jimin Sun *, Zhenqing Zhang

Key Laboratory of Cenozoic Geology and Environment, Institute of Geology and Geophysics, Chinese Academy of Sciences, P. O. Box 9825, Beijing 100029, China

ARTICLE INFO

ABSTRACT

Thick Cenozoic deposits were shed into the foreland basin of the Tian Shan Range, providing great potential for understanding the relationship between tectonic history and paleoclimatic changes. In the present study, we compiled a pollen record for the interval 26.5–2.6 Ma based on a palynological analysis of a latest Oligocene–Pliocene stratigraphic sequence in the northern foreland basin of the Tian Shan. Our results indicate that a remarkable warm climate occurred at ca. 18–15 Ma ago, corresponding to the Mid-Miocene Climatic Optimum, while a change to an arid climate occurred at 6 Ma, marked by an increase in the drought-tolerant herb taxa *Artemisia* and Chenopodiaceae. This latter change was coincident with the late Cenozoic climatic deterioration recorded at high latitudes in the Northern Hemisphere. These inferred climatic events are further supported by the results of principal component analysis of the pollen data, such records are important archives in reconstructing the paleoclimate of the Asian interior.

1. Introduction

Earth's climate changed during the Cenozoic from an ice-free, warm climate to a cold climate marked by the development of massive continental ice sheets. The details of this climate change have been reconstructed using composite high-resolution deep-sea oxygen isotope records (e.g., Miller et al., 1987; Zachos et al., 2001). Many significant warm and cool climatic events occurred during the stepwise Cenozoic cooling process. One of the most intriguing climatic events of the Neogene was the Middle Miocene (~15–18 Ma) global warming known as the Mid-Miocene Climatic Optimum (e.g., Flower and Kennett, 1994); subsequent to this event, the earth's climate showed a gradual cooling, with the increasing global ice volumes (Shackleton and Kennett, 1975; Escutia et al., 2005).

In contrast to deep-sea sediments, terrestrial deposits usually record hiatuses in deposition. It is difficult to find a single continuous sequence of deposits covering the entire Cenozoic. Among the various parameters used in reconstructing long-term terrestrial climate change, pollen analysis is one of the most useful because vegetation type shows a direct relation with climate change. In China, many recent studies have investigated the palynology of Neogene sediments (e.g., Wang, 1990; Wang et al., 1990; Hu and Sarjeant, 1992; Liu and Leopold, 1994; Ma et al., 1998, 2004; Liang et al., 2003; Sun and Wang, 2005; Sun et al., 2007; Xu et al., 2008), however, the long-term paleoclimate records of the thick Cenozoic deposits of the northern foreland basins of the Tian Shan Range remain to be studied in detail.

In this context, the objectives of the present work are to: (1) present pollen record for the Tian Shan region from the latest Oligocene to early Pleistocene, and (2) discuss climate change over this period based on our palynological data.

2. Regional setting

The Tian Shan Range is one of the longest mountain ranges in Central Asia, stretching more than 2500 km from Tashkent (Uzbekistan) in the west to northwestern China in the east (Fig. 1a). The average elevation of ridges along the range is about 4000 m above sea level (asl), while the highest summits exceed 7400 masl. Geologically, the range is a Paleozoic fold belt (e.g., Allen et al., 1992; Gao et al., 1998) that was eroded during the Mesozoic (Deng et al., 2000). The range was strongly reactivated during the Cenozoic as a result of intracontinental deformation associated with the India–Eurasia convergent system (e.g., Avouac et al., 1993; Hendrix et al., 1994; Yin et al., 1998; Burchfiel et al., 1999; Deng et al., 2000; Fu et al., 2003; Sun et al., 2004). In response to N–S crustal shortening during the Cenozoic, thick Cenozoic sediments were folded to form three relatively low-lying ranges oriented parallel to the E–W trend of the main Tian Shan Range. The Cenozoic deposits in the northern foreland basins of the Tian Shan are up to 5000 m thick, and are exposed where a series of northward-flowing rivers transect the basins. The section considered in the present study is exposed along the Taxihe River (Fig. 1b), where Cenozoic deposits can be observed at elevations ranging from about 800 to 1300 masl.

The studied deposits are part of the Tugulu Anticline (Fig. 2a), an overturned fold (Fig. 2b) some 50 km long and 10–15 km wide. The best exposures are found along the Taxihe River (transect A–B in

---

* Corresponding author. Tel.: +86 10 8299 8389; fax: +86 10 6201 0846.
E-mail address: jmsun@mail.igcas.ac.cn (J. Sun).
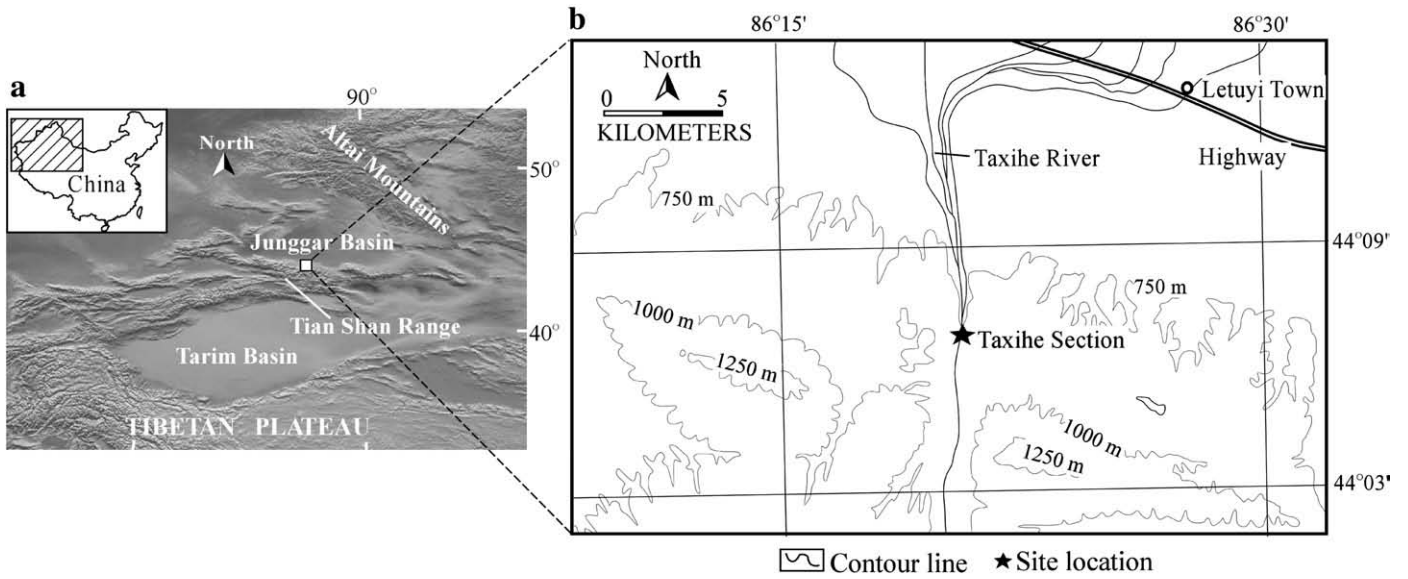
Fig. 1. Digital elevation model image of the Tian Shan Range and surrounding region (a) and topographic map of the study area (b).

Fig. 2a). The studied part of the section consists of grey lacustrine mudstone of the Oligocene Anjihaihe Formation (E_{3A}), reddish mudstone of the latest Oligocene Shawan Formation (E_{3S}), dominant lacustrine mudstone of the Miocene Taxihe Formation (N_{1T}), alternations of grey gravels and brownish siltstone of the Pliocene Dushanzi Formation (N_{2D}), and the coarse molasse deposits of the early
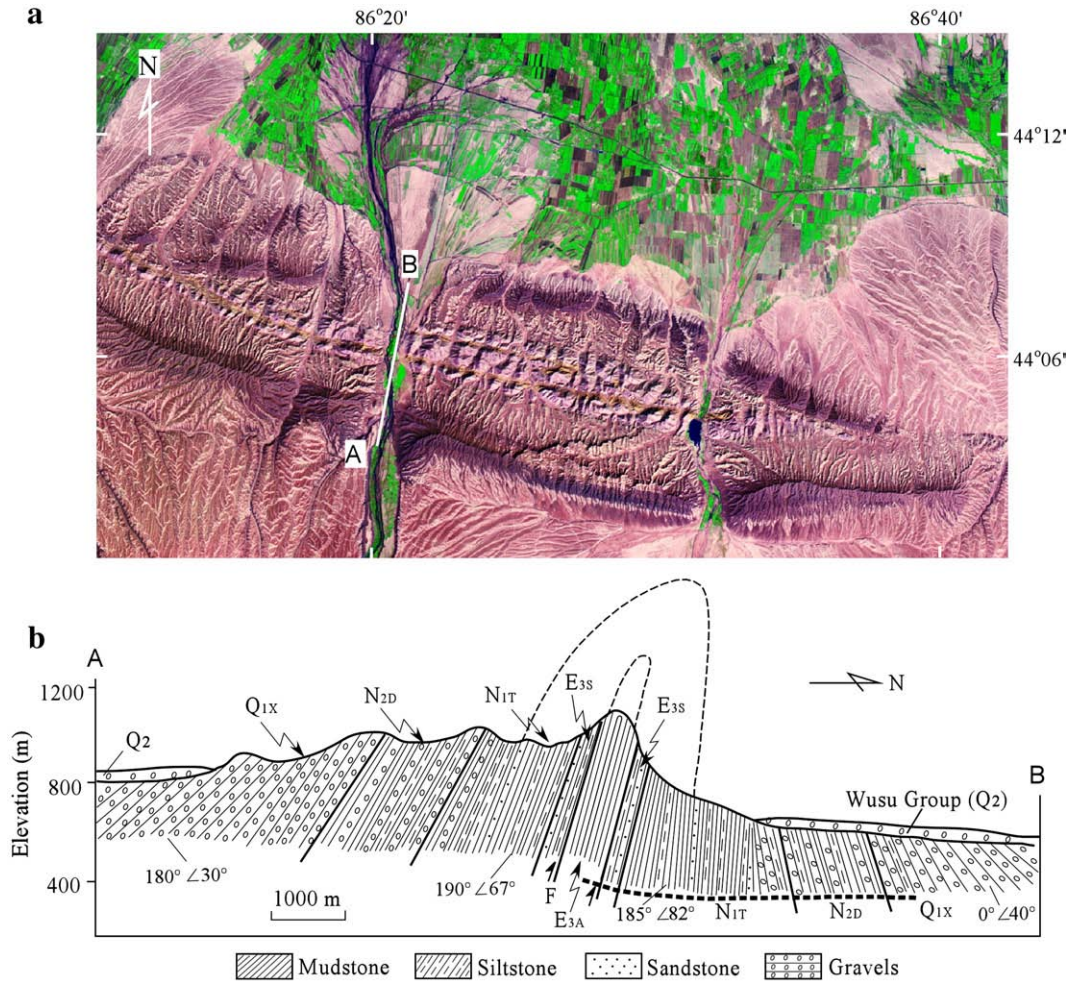
Fig. 2. (a) Landsat image of the Tugulu Anticline, and (b) the exposed Cenozoic strata of the Tugulu Anticline along cross-section A–B, cut by the Taxihe River. The bold dashed line in the lower part of (b) shows the sampling route. E_{3A}: Oligocene Anjihai Formation; E_{3S}: Late Oligocene Shawan Formation; N_{1T}: Miocene Taxihe Formation; N_{2D}: Pliocene Dushanzi Formation; Q_{1X}: Early Pleistocene Xiyu Formation; Q_2: Middle Pleistocene; F: Thrust fault.
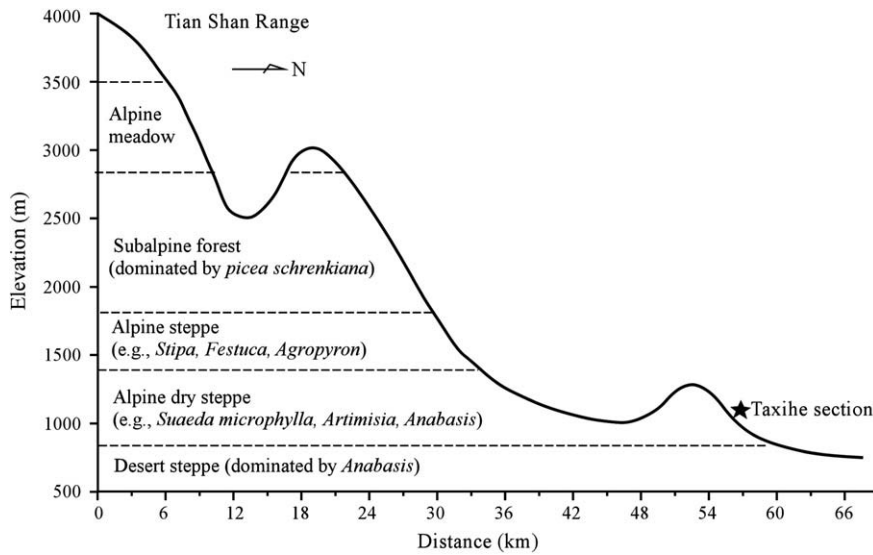
Fig. 3. Present-day vertical distribution of vegetation belts upon the northern slopes of the Tian Shan Range.

Pleistocene Xiyu Formation (Q_{1X}) (Fig. 2b). The dominant lithology changes from distal fine-grained lacustrine mudstone during the Late Oligocene and Miocene to proximal coarse molasse deposits since the latest Miocene. These strata are folded and unconformably overlain by the Middle Pleistocene (Q_2) Wusu Group (Fig. 2b).

Although the Tian Shan Range is located in an arid part of Central Asia, it is high enough to intercept moist air masses that originate from the Arctic and Atlantic oceans. The annual precipitation ranges from 100–200 mm at lower elevations to 400–800 mm at higher elevations. In the study region, the present-day mean annual temperature is 6.9°C, and orogenic precipitation is sufficient to support a diverse range of vegetation at different altitudes on north-facing slopes (Fig. 3): alpine meadows occur at elevations of 2800–3500 masl, subalpine conifer forest dominated by *Picea schrenkiana* occurs at elevations of 1800–2800 masl, alpine steppe dominated by *Stipa*, *Festuca*, and *Agropyron* occurs at 1400–1800 masl, dry steppe dominated by *Artemisia*, *Suaeda,* and *Anabasis* occurs at elevations of 800–1400 masl, and desert steppe dominated by *Anabasis* occurs below 800 masl.

3. Materials and methods

We collected 192 samples from the 2980 m thick Taxihe section for palynological analysis, with an average sampling interval of ~15 m. Because our previous study of the late Cenozoic pollen record of the northern Tian Shan revealed that pollen concentrations are generally low, with some samples even being barren (Sun et al., 2007), in the present study we analyzed approximately 150 g of sediment from each sample. Samples were treated with HCl (35%) and HF (70%) to remove carbonates and silica. Separation of the palynomorphs from the residue was carried out using $ZnCl_2$ (density=2), following the method of Faegri and Iversen (1989). Sieving was performed using a 10-μm nylon sieve. Slides were prepared by mounting the pollen grains in glycerin jelly, pollen were then counted under a microscope.

Thermal demagnetization experiment was performed on 551 orientated samples to obtain magnetostratigraphic data, using a 2G three-axis cryogenic magnetometer housed in field-free space (<300 nT) at the Institute of Geology and Geophysics, Chinese Academy of Sciences.

We also performed a principal components analysis (PCA) of the pollen data, which is an indirect ordination technique for obtaining a low-dimensional representation of multivariate data such that the data can be explored visually in a two-dimension PCA correlation biplot and any structure in the data identified. In this study, pollen taxa reaching 2% or greater were included in the PCA analysis.

4. Results

A total of 66 pollen taxa were identified (Table 1), the raw counts of the dominant species within each sample are listed in Table 2.

Although both lithology and sedimentary facies may affect pollen counts, our counts do not change significantly with depth (Fig. 4).

Table 1
List of the taxa identified in this study

Gymnospermous pollen	Angiospermous pollen (continued)
Podocarpus	Morus
Dacrydium	Tilia
Pinus	Salix
Abies	Oleaceae
Picea	Corylus
Cycas	Artemisia
Ginkgo	Aster
Tsuga	Compositae
Cupressaceae	Chenopodiaceae
Keteleeria	Ranunculaceae
Cedrus	Umbelliferae
Larix	Polygonum
Ephedra	Thalictrum
Angiospermous pollen	Ericaceae
Betula	Sanguisorba
Carpinus	Humulus
Alnus	Potamogeton
Quercus	Typha
Castanea	Elaeagnaceae
Juglans	Geraniaceae
Pterocarya	Cyperaceae
Carya	Gramineae
Ulmus	*Pteridophyte pollen*
Zelkova	Lycopodium
Celtis	Selaginella
Hemiptelea	Polypodium
Meliaceae	Polypodiaceae
Acer	Pteris
Liquidambar	Hymenophyllum
Myrica	Lygodium
Rosaceae	Adiantum
Rutaceae	Cyatheaceae
Magnoliaceae	Hicriopteris
Aquifoliaceae	Filicales

Table 2
Raw counts of the dominant pollen species in each sample

Depth (m)	Abies	Picea	Tsuga	Cedrus	Pinus	Podocarpus	Betula	Carpinus	Alnus	Quercus	Castanea	Juglans	Pterocarya	Carya
0	20	2	0	0	203	0	33	1	1	3	0	1	0	1
20	25	3	0	0	163	1	44	0	0	2	0	10	0	0
32	27	1	0	0	184	0	39	1	1	1	0	3	0	0
43	23	2	1	0	150	0	50	0	1	2	0	6	0	0
59	24	0	0	1	181	0	49	1	0	5	0	9	1	0
67	23	0	0	0	162	0	75	2	0	1	0	8	0	1
79	24	1	0	0	205	0	41	0	1	2	0	4	0	1
93	26	2	0	0	164	0	45	2	0	4	0	4	1	1
108	32	2	0	2	191	0	43	2	0	3	0	3	0	0
120	22	1	0	0	165	2	58	1	1	2	1	9	0	1
151	24	1	0	0	148	0	43	2	0	4	0	3	0	1
160	17	2	0	1	121	0	56	1	2	2	0	2	0	0
168	23	1	0	0	133	0	41	3	0	2	0	4	0	1
177	22	2	0	0	153	0	47	0	0	4	0	6	1	0
197	23	1	0	0	156	0	43	1	0	1	0	7	0	0
208	22	0	0	0	147	0	49	1	0	2	0	4	0	0
224	13	1	0	0	143	0	59	2	0	2	0	5	0	0
240	18	1	0	0	127	0	51	2	0	3	0	3	0	0
253	27	2	0	0	141	0	53	3	1	6	0	6	0	0
287	19	2	0	0	151	0	54	2	0	1	1	5	0	0
299	24	1	0	0	141	0	67	2	0	4	0	3	1	0
320	22	1	0	0	160	0	41	2	0	2	0	6	0	1
334	22	0	0	0	130	1	51	1	0	1	0	2	0	0
340	18	2	0	0	165	1	59	2	0	4	0	3	1	0
352	21	1	0	0	153	0	74	0	4	1	0	3	2	0
362	23	0	0	1	139	1	54	3	0	3	0	5	0	1
377	24	1	0	1	130	0	55	1	0	4	0	3	0	1
394	25	1	1	0	156	0	46	0	1	1	0	2	0	0
404	20	0	0	0	139	0	49	2	0	1	0	3	0	1
417	19	0	0	0	163	0	59	1	0	3	0	4	0	0
427	21	1	0	0	172	0	69	1	0	2	0	3	0	0
455	24	1	0	0	182	0	58	1	0	4	0	3	0	0
460	23	0	0	0	177	1	52	1	0	5	0	3	0	0
468	22	1	0	0	175	1	55	2	1	2	0	7	0	0
479	24	0	0	0	178	0	44	1	0	4	0	6	0	1
494	22	0	0	0	159	1	62	1	1	2	0	3	0	0
512	21	1	0	0	179	0	49	3	0	1	0	6	0	0
523	25	0	0	0	164	1	56	1	0	5	0	5	1	1
541	16	1	0	0	176	0	49	1	0	2	0	4	0	0
562	21	1	0	0	168	0	52	2	0	1	0	1	0	0
605	18	0	0	0	145	2	63	1	0	4	0	2	1	0
613	22	1	0	0	145	0	58	0	1	5	0	7	1	1
626	22	1	0	0	163	0	51	1	0	2	0	3	1	0
642	13	0	1	0	141	0	55	0	0	6	0	6	0	0
655	9	2	0	0	88	1	42	0	0	2	0	2	1	0
672	13	1	0	0	119	0	42	1	0	2	0	1	1	0
688	11	0	0	0	101	0	41	0	0	1	0	1	1	0
702	11	1	0	0	125	0	27	1	0	3	0	5	0	2
717	12	0	0	0	124	0	42	2	0	2	0	2	0	1
730	15	0	0	0	166	0	40	1	0	2	0	2	1	0
748	18	1	0	0	153	0	34	2	0	2	0	5	0	0
759	19	0	0	0	115	0	38	0	0	6	0	4	0	0
789	10	1	0	0	141	1	35	0	0	0	0	2	0	0
818	15	0	0	0	101	0	37	0	0	2	0	5	0	1
829	12	0	0	0	111	0	36	2	0	2	0	1	0	0
842	8	1	1	0	171	0	40	0	0	4	0	3	0	2
856	17	0	0	0	131	1	36	1	1	3	0	5	1	0
876	12	1	0	0	123	0	35	1	1	2	0	1	0	1
892	18	0	1	0	119	0	45	3	1	6	0	4	0	1
908	19	2	1	0	122	0	71	2	0	2	0	4	0	0
916	9	0	0	0	135	0	40	0	0	1	0	4	2	0
931	19	0	0	0	146	0	51	0	0	1	0	5	0	3
948	8	0	0	0	146	0	49	3	0	5	0	6	0	0
963	13	1	0	0	138	0	48	0	0	2	0	6	1	0
981	15	1	0	0	147	0	56	2	1	6	0	5	0	1
994	25	0	0	0	168	0	44	2	0	5	0	7	1	0
1008	20	1	0	0	160	0	53	3	0	1	0	3	0	0
1027	18	0	0	0	135	0	52	1	0	5	0	5	1	0
1043	17	2	0	0	137	0	37	2	0	1	1	4	1	0
1055	21	1	0	0	179	1	51	2	0	2	0	6	0	0
1068	13	1	0	0	141	0	42	2	1	2	0	4	0	1
1085	14	1	0	0	137	0	48	2	0	1	0	2	1	0
1105	13	0	0	0	165	1	38	1	0	4	0	4	1	0
1124	15	0	0	0	141	0	33	1	0	1	0	5	0	0

Table 2 (continued)

Depth (m)	Abies	Picea	Tsuga	Cedrus	Pinus	Podocarpus	Betula	Carpinus	Alnus	Quercus	Castanea	Juglans	Pterocarya	Carya
1138	13	0	0	0	137	1	50	4	1	2	1	4	0	0
1165	18	1	0	0	170	2	52	1	1	1	1	4	0	0
1175	11	0	0	0	143	2	65	1	0	2	0	4	0	1
1200	13	1	0	0	147	0	54	2	1	2	6	3	1	0
1214	19	1	0	1	153	0	59	1	0	2	1	3	1	0
1228	12	1	0	0	140	0	49	1	0	3	0	11	0	1
1244	24	1	0	0	170	0	45	3	0	1	0	3	0	0
1266	23	3	0	0	160	1	47	0	0	4	0	6	0	0
1290	16	1	0	0	142	0	46	2	0	2	0	5	0	0
1304	17	2	0	0	135	1	48	0	0	3	0	3	0	1
1327	21	1	0	0	143	1	45	1	0	3	1	3	1	0
1354	15	0	0	0	145	0	58	3	0	4	0	4	1	1
1366	18	0	0	0	142	0	46	0	2	4	1	5	1	0
1386	13	1	0	0	153	0	51	2	0	3	1	7	0	1
1411	19	1	0	0	163	0	59	2	0	5	1	4	0	0
1439	18	0	0	0	141	0	51	1	1	1	1	2	0	0
1455	22	1	0	1	149	0	57	2	0	1	1	6	0	0
1475	11	0	1	0	151	0	35	7	1	3	0	3	0	0
1495	8	1	0	0	138	0	59	1	1	3	0	5	1	1
1508	7	0	0	0	125	0	46	1	0	2	1	4	0	1
1522	5	1	0	0	126	0	54	0	0	2	1	7	0	1
1538	13	0	0	1	151	0	79	2	0	8	0	8	1	0
1554	8	1	0	1	140	0	71	1	0	6	0	12	1	1
1570	2	0	0	0	112	0	61	3	0	3	0	9	2	1
1581	1	0	0	0	94	0	64	0	0	2	0	6	1	1
112	3	0	0	0	94	1	51	2	0	5	0	6	2	1
1628	2	1	0	0	109	0	61	1	1	3	0	9	1	1
1644	4	0	0	0	113	0	63	2	1	4	0	8	1	1
1657	2	1	0	0	102	1	70	1	0	5	0	9	2	2
1674	2	1	0	0	90	1	55	0	2	3	0	9	1	2
186	6	1	0	0	105	1	72	1	0	5	0	13	5	1
1701	4	1	0	0	102	0	75	1	0	7	1	10	2	1
1713	5	0	0	0	125	0	83	1	0	6	0	9	2	1
1744	4	0	0	0	94	0	77	3	0	3	0	9	1	2
156	4	1	0	0	141	0	88	2	0	6	0	12	0	0
1764	2	0	0	0	87	1	66	1	2	3	0	7	1	1
1779	4	1	0	0	104	1	74	0	1	4	0	7	1	1
1793	4	1	0	0	116	1	84	2	0	7	0	7	0	2
1807	4	1	0	0	141	1	79	0	1	3	0	7	1	1
117	3	0	0	0	119	0	90	1	0	4	0	9	1	2
1835	3	3	0	0	95	1	63	1	0	0	0	7	0	1
1846	0	1	0	0	78	0	64	1	0	3	1	8	1	0
1888	1	0	0	0	76	1	75	0	0	4	0	8	1	1
1894	1	0	0	1	121	0	82	3	0	5	0	17	0	1
106	4	0	0	0	96	0	95	3	0	12	0	11	0	3
1927	7	0	0	0	116	2	83	0	1	4	0	12	3	1
1942	6	0	0	0	130	0	83	1	1	4	0	5	1	0
1955	11	1	0	0	127	1	70	1	1	7	0	5	0	0
1978	18	0	0	0	150	0	60	1	1	3	0	8	0	0
1989	5	0	0	0	119	0	77	2	1	4	0	11	0	1
2007	8	0	0	0	117	0	75	1	2	2	0	5	0	1
2021	7	1	0	0	85	0	72	2	2	3	0	3	1	1
2041	1	0	0	0	104	1	38	2	0	4	0	4	0	1
2048	12	0	0	0	115	0	51	1	1	1	0	6	0	2
2071	9	0	0	0	113	0	69	2	9	4	0	1	0	0
2089	2	0	0	0	88	1	51	3	1	2	0	9	2	0
2101	16	0	0	0	103	1	49	2	0	3	0	3	0	0
2115	16	0	0	0	142	0	65	1	0	2	0	5	0	0
2124	9	1	0	0	149	0	55	1	0	2	0	7	0	1
2133	17	1	0	0	148	0	56	0	1	2	0	10	0	1
2151	7	0	0	0	94	0	42	0	0	3	0	3	0	0
2160	7	1	0	0	93	0	63	1	0	2	0	4	0	0
2167	5	0	0	0	93	0	54	1	1	3	0	10	0	1
2169	5	1	0	0	132	0	49	0	0	1	0	4	0	1
2179	5	0	0	0	98	0	48	1	2	1	0	4	1	1
2190	9	1	0	0	134	0	72	2	0	2	0	4	0	2
2196	15	1	0	0	133	1	64	2	1	4	0	5	0	2
2207	9	0	0	0	172	0	89	1	0	4	0	4	1	0
2219	12	0	0	0	143	0	58	1	0	2	0	6	0	1
2235	3	0	8	0	113	0	48	1	1	2	0	4	0	1
2254	7	0	0	0	137	1	35	1	2	1	0	6	0	0
2269	12	1	0	0	120	2	54	1	3	3	0	4	0	0
2281	11	1	0	0	115	1	53	0	0	4	0	7	0	1
2294	13	0	0	0	134	0	39	0	1	1	0	9	1	0

Table 2 (continued)

Depth (m)	Abies	Picea	Tsuga	Cedrus	Pinus	Podocarpus	Betula	Carpinus	Alnus	Quercus	Castanea	Juglans	Pterocarya	Carya
2306	11	0	0	0	110	0	46	1	3	2	0	5	0	0
2368	8	0	0	0	127	0	50	1	0	2	0	8	0	1
2376	19	0	0	2	114	0	56	2	0	4	0	7	0	0
2388	12	1	0	0	137	1	59	1	0	2	0	5	0	1
2403	3	0	0	0	87	0	46	0	0	0	0	7	1	1
2426	8	0	0	1	93	0	58	0	1	2	0	7	0	1
2435	11	0	0	0	113	0	32	1	0	2	0	2	0	0
2468	16	1	0	0	131	0	39	2	1	3	0	7	1	0
2480	6	0	0	0	94	0	35	1	0	1	0	7	1	1
2489	22	2	1	0	141	1	58	1	0	1	1	8	0	2
2498	7	1	0	0	84	0	32	2	0	0	0	2	0	1
2504	9	0	0	0	105	0	36	1	0	0	0	1	0	0
2509	7	0	0	0	128	0	38	1	2	1	0	4	0	0
2517	7	0	0	0	122	0	29	1	0	1	0	3	0	1
2527	9	1	3	0	94	1	29	1	0	1	0	3	1	1
2530	18	0	0	0	160	0	36	1	1	1	0	5	0	0
2549	15	1	0	0	124	0	52	0	0	1	0	3	0	1
2560	23	1	0	0	144	0	38	0	0	1	0	4	0	0
2574	26	1	0	0	158	0	61	0	0	5	0	8	3	0
2593	25	1	0	0	165	1	43	1	0	3	0	3	0	0
2616	16	1	0	0	143	0	54	1	1	4	0	4	0	0
2635	12	0	0	0	123	0	37	1	0	1	0	3	0	0
2652	13	0	0	0	124	0	35	2	0	1	0	2	0	0
2661	14	0	0	0	148	0	42	1	1	1	0	0	0	0
2684	16	1	0	0	141	0	50	1	0	4	0	3	0	0
2701	12	0	0	0	143	0	42	0	2	3	0	2	0	0
2717	6	1	0	0	86	1	38	1	1	1	0	1	1	1
2733	14	0	0	0	115	0	54	1	0	2	0	8	0	1
2742	13	1	1	0	105	0	51	0	0	3	0	6	0	0
2752	7	1	0	0	122	0	38	1	0	0	1	3	0	1
2762	23	1	0	1	162	0	52	0	1	1	0	6	0	0
2776	18	1	0	0	140	0	62	2	0	7	0	7	1	0
2790	21	0	1	0	136	0	52	2	0	4	0	1	0	1
2802	18	3	0	0	170	0	63	1	0	3	0	6	0	1
2818	17	0	0	0	193	0	56	0	0	6	0	4	0	1
2831	19	1	0	0	129	1	39	1	0	3	1	3	1	0
2874	27	0	0	0	175	0	38	1	0	4	0	6	0	1
2893	8	0	0	0	119	1	57	1	0	3	0	2	0	1
2917	13	0	0	0	101	0	41	1	0	3	0	3	1	0
2938	11	2	0	0	121	0	39	1	0	2	0	3	0	1
2950	22	0	0	0	158	1	35	0	0	1	0	6	0	0
2960	4	1	0	0	33	0	11	1	0	0	0	1	0	0
2965	23	1	0	0	131	0	44	1	1	2	0	2	0	0
2980	25	1	0	0	136	1	33	1	0	1	0	2	0	0

Depth (m)	Ulmus	Tilia	Corylus	Ephedra	Artemisia	Compositae	Chenopodiaceae	Gramineae	Lycopodium	Selaginella	Polypodiaceae
0	0	3	1	0	8	1	2	0	0	1	1
20	0	4	2	0	8	1	1	0	0	1	3
32	1	2	2	1	4	1	1	0	0	0	0
43	1	3	5	0	3	0	1	0	0	1	0
59	2	3	3	1	8	1	2	0	0	0	1
67	2	0	2	1	6	1	1	0	0	1	1
79	1	4	2	0	5	0	1	0	1	0	2
93	0	8	2	0	4	0	1	1	0	0	2
108	1	3	2	1	6	1	1	0	0	1	6
120	1	4	5	1	5	0	0	0	0	0	4
151	2	8	3	0	3	0	1	0	0	1	1
160	1	2	3	0	8	0	2	1	0	0	1
168	0	2	2	2	3	1	2	0	0	0	2
177	1	3	4	1	4	1	0	0	0	0	2
197	0	4	2	0	4	1	1	0	0	0	1
208	0	2	5	2	6	1	1	0	0	1	3
224	2	1	3	1	4	1	1	0	0	1	1
240	2	2	4	0	9	0	0	0	1	1	2
253	1	4	3	0	4	0	1	0	0	1	2
287	0	5	3	1	5	1	1	1	0	1	2
299	0	2	4	1	2	1	0	0	0	1	3
320	1	4	2	0	7	1	1	0	0	0	1
334	2	3	1	0	6	1	1	0	0	1	2
340	1	5	5	0	7	1	1	0	0	0	1
352	0	1	8	0	11	0	1	0	0	0	2
362	2	3	7	0	6	0	1	0	0	1	1
377	2	3	3	0	8	1	1	1	0	1	2
394	0	4	4	0	25	0	10	3	0	0	2
404	1	2	2	0	3	0	1	0	0	1	1

Table 2 (*continued*)

Depth (m)	Ulmus	Tilia	Corylus	Ephedra	Artemisia	Compositae	Chenopodiaceae	Gramineae	Lycopodium	Selaginella	Polypodiaceae
417	2	3	6	0	4	1	1	0	1	0	1
427	1	1	3	0	3	1	0	0	0	1	1
455	1	1	2	0	3	1	0	0	0	1	1
460	1	2	3	0	4	1	1	0	0	1	1
468	0	4	6	0	3	0	1	0	0	1	0
479	0	3	3	0	5	1	0	0	2	0	1
494	1	4	1	0	4	1	0	0	0	1	3
512	2	9	3	0	3	1	0	0	0	1	2
523	0	7	7	0	4	1	1	1	0	0	0
541	1	4	2	0	5	0	2	0	0	1	0
562	1	3	3	1	2	1	1	0	1	1	0
605	2	3	2	0	6	2	1	0	0	1	2
613	0	5	2	0	7	1	2	0	0	1	1
626	0	4	1	1	7	1	2	0	0	1	1
642	1	4	2	0	21	1	6	0	2	2	2
655	1	5	3	0	24	1	5	0	0	2	2
672	1	2	1	0	16	0	4	0	0	1	1
688	1	1	1	0	15	2	4	1	0	1	2
702	3	3	2	0	14	0	3	3	0	1	3
717	2	7	0	1	13	1	7	1	0	0	3
730	1	3	4	0	22	1	5	0	0	1	4
748	1	4	3	2	19	2	6	0	0	2	1
759	2	5	1	1	16	1	5	0	0	0	2
789	1	8	0	0	15	1	3	1	0	2	1
818	1	2	2	3	9	2	5	0	0	0	1
829	1	4	4	1	18	0	2	0	0	1	4
842	3	5	2	1	14	1	10	2	0	2	3
856	1	5	2	0	14	0	3	2	0	1	1
876	0	3	1	0	18	0	5	0	1	1	1
892	2	4	4	1	36	2	3	1	0	0	6
908	1	5	3	0	25	1	6	2	0	0	3
916	1	1	3	0	12	1	3	0	0	0	2
931	3	3	3	1	2	1	1	1	1	1	4
948	1	4	1	2	5	1	3	0	0	0	1
963	1	1	2	0	3	0	1	0	0	0	1
981	0	2	2	1	4	0	1	0	0	1	2
994	2	5	3	0	6	1	1	0	0	1	1
1008	2	4	2	0	4	2	2	0	0	0	2
1027	1	3	2	0	2	1	1	0	0	1	1
1043	1	4	2	0	2	0	1	0	0	0	1
1055	1	4	3	0	2	0	0	0	0	0	2
1068	1	2	2	1	2	1	1	0	0	0	1
1085	1	7	1	0	2	1	1	0	0	1	1
1105	1	6	3	0	2	0	0	0	0	1	1
1124	2	2	1	0	2	1	1	0	0	1	2
1138	4	3	4	1	2	0	1	1	0	0	3
1165	0	9	4	0	2	0	1	0	0	1	1
1175	4	2	3	1	3	0	0	0	0	2	1
1200	0	3	4	0	3	1	1	0	0	1	2
1214	1	4	3	1	2	1	1	0	0	0	1
1228	1	5	1	2	2	0	0	0	0	0	0
1244	0	2	2	1	2	0	2	0	0	1	2
1266	1	2	3	2	2	0	1	0	0	0	5
1290	0	8	3	1	3	1	1	0	0	0	1
1304	0	7	5	0	3	0	1	0	0	1	1
1327	0	6	1	0	2	0	1	0	0	1	1
1354	2	4	1	0	4	1	1	1	0	1	2
1366	1	0	2	1	3	0	1	0	0	1	1
1386	2	3	2	0	2	1	1	1	0	1	2
1411	2	6	2	2	3	1	0	0	0	0	1
1439	1	3	1	0	3	0	1	1	0	1	1
1455	1	5	2	1	3	1	1	1	0	1	0
1475	0	4	3	1	2	0	0	0	0	1	1
1495	3	3	4	0	2	0	0	1	0	0	1
1508	1	2	1	0	2	0	0	0	0	1	1
1522	1	3	2	0	2	2	1	0	0	1	4
1538	2	4	3	0	3	1	1	1	0	1	2
1554	3	4	4	2	3	0	1	0	0	1	3
1570	3	3	5	0	2	0	1	1	0	1	1
1581	4	4	3	0	2	0	1	0	0	1	2
1612	1	4	3	1	1	0	1	0	0	0	2
1628	1	4	3	0	1	0	0	1	0	0	2
1644	1	2	2	1	2	0	1	0	0	0	2
1657	1	8	1	0	2	0	0	0	0	0	0
1674	1	3	2	1	2	0	1	1	0	0	1
1686	5	3	2	0	1	0	0	1	1	0	1

Table 2 (*continued*)

Depth (m)	Ulmus	Tilia	Corylus	Ephedra	Artemisia	Compositae	Chenopodiaceae	Gramineae	Lycopodium	Selaginella	Polypodiaceae
1701	1	5	1	0	4	0	2	0	0	0	3
1713	4	6	1	0	4	0	2	1	0	0	2
1744	1	5	3	0	4	0	1	1	0	0	1
1756	4	9	5	2	1	0	0	0	1	0	3
1764	3	2	4	1	1	0	0	1	0	0	1
1779	2	4	1	0	1	0	1	1	0	0	1
1793	2	3	3	0	1	0	0	1	0	0	1
1807	2	1	0	0	3	0	1	1	0	0	3
1817	0	1	2	1	2	1	0	0	0	0	1
1835	1	1	2	1	3	0	1	0	0	0	1
1846	2	0	1	2	2	0	1	0	0	0	2
1888	1	4	1	0	2	0	1	0	0	0	1
1894	3	2	1	0	3	0	2	0	0	0	2
1906	2	4	3	1	1	0	0	0	0	0	3
1927	4	3	4	1	2	0	4	1	0	0	3
1942	3	4	2	0	3	0	1	0	0	0	2
1955	1	5	4	0	1	1	1	1	0	0	1
1978	1	5	2	0	4	1	1	0	0	1	1
1989	1	5	1	1	5	0	1	0	0	0	1
2007	1	9	4	0	3	0	0	0	0	0	3
2021	0	3	4	0	5	2	1	0	0	0	1
2041	1	3	2	0	3	0	1	0	0	1	1
2048	1	8	2	0	2	1	1	0	0	1	4
2071	0	4	2	0	1	2	2	0	0	0	1
2089	0	2	3	0	1	0	0	0	0	1	1
2101	1	1	3	1	2	0	0	0	0	1	2
2115	1	6	2	0	1	1	1	0	1	1	0
2124	1	3	1	0	3	1	1	0	1	1	2
2133	1	1	7	0	3	0	0	0	0	0	0
2151	1	5	2	0	3	0	1	1	1	0	1
2160	2	3	1	0	3	1	1	0	0	0	1
2167	2	6	1	1	3	0	1	0	0	0	1
2169	2	8	3	0	5	0	2	1	0	0	1
2179	0	4	0	0	1	0	1	0	0	0	1
2190	2	2	3	0	7	1	1	0	0	0	2
2196	1	4	5	0	2	0	1	0	0	0	1
2207	1	2	4	1	0	0	2	0	0	0	1
2219	2	5	2	1	2	1	5	1	0	0	1
2235	1	2	2	1	1	0	0	0	0	0	2
2254	1	2	2	0	5	0	5	1	0	0	1
2269	2	1	4	0	3	0	3	0	0	0	1
2281	0	2	4	0	3	0	1	0	0	0	2
2294	5	5	1	2	2	0	10	1	0	0	1
2306	1	3	4	0	3	0	5	0	0	0	1
2368	3	6	2	0	4	0	1	0	0	0	1
2376	3	4	0	2	6	0	2	0	0	0	1
2388	0	5	3	0	4	0	3	0	0	1	3
2403	2	3	2	1	5	0	5	0	0	0	1
2426	1	2	3	0	3	0	1	1	0	1	3
2435	1	3	2	0	2	1	13	0	0	1	1
2468	3	10	3	0	5	0	1	1	0	1	1
2480	0	11	3	1	1	0	0	0	0	1	1
2489	0	5	2	1	4	0	1	0	0	1	1
2498	0	1	1	1	2	1	1	0	0	1	2
2504	2	4	3	1	3	0	6	0	1	1	1
2509	1	1	1	0	5	1	2	0	0	2	1
2517	1	2	3	1	4	0	1	0	0	1	1
2527	0	3	1	1	1	0	2	1	0	1	0
2530	2	1	2	3	5	0	44	1	0	2	1
2549	1	3	1	0	4	0	3	0	1	0	1
2560	0	4	3	1	3	1	2	1	0	1	1
2574	2	4	4	0	3	1	1	0	0	0	2
2593	0	3	1	0	4	2	2	1	0	1	0
2616	0	4	0	1	2	0	1	0	0	0	2
2635	0	4	1	0	3	2	1	1	0	2	1
2652	1	4	2	1	2	0	1	1	0	1	1
2661	1	5	2	0	2	1	4	0	0	1	3
2684	0	3	1	3	5	1	2	0	0	0	1
2701	2	4	1	0	2	0	0	0	1	0	1
2717	1	2	2	0	3	0	1	0	0	0	2
2733	1	6	1	2	3	0	1	1	0	1	2
2742	2	2	3	1	2	1	2	1	1	0	2
2752	2	2	1	0	2	0	2	0	0	1	1
2762	1	6	3	0	5	2	1	1	1	0	2
2776	3	2	6	0	4	1	3	1	0	0	1
2790	0	8	2	1	3	1	2	0	0	1	5

Table 2 (*continued*)

Depth (m)	Ulmus	Tilia	Corylus	Ephedra	Artemisia	Compositae	Chenopodiaceae	Gramineae	Lycopodium	Selaginella	Polypodiaceae
2802	0	8	2	0	2	0	2	1	0	1	2
2818	1	2	3	1	3	0	3	0	0	2	2
2831	2	2	3	3	1	0	4	0	1	1	2
2874	0	7	2	1	1	0	1	0	0	0	2
2893	1	4	1	0	2	0	1	1	0	1	0
2917	3	3	3	0	0	0	0	0	0	1	2
2938	1	3	3	2	0	0	8	0	0	0	1
2950	1	5	1	0	0	1	2	1	0	0	0
2960	0	0	2	23	0	1	3	0	0	1	0
2965	1	4	3	3	0	1	4	1	0	1	1
2980	1	0	2	2	0	3	3	0	0	1	1

samples have pollen counts of between 220 and 260 (average, 234). Therefore, we found little effect of lithofacies type on pollen preservation, meaning that the pollen assemblages are likely to mainly reflect paleoclimate. The major floral components are shown in a pollen percentage diagram (Fig. 5), photographs of selected pollen grains are provided in Figs. 6 and 7.
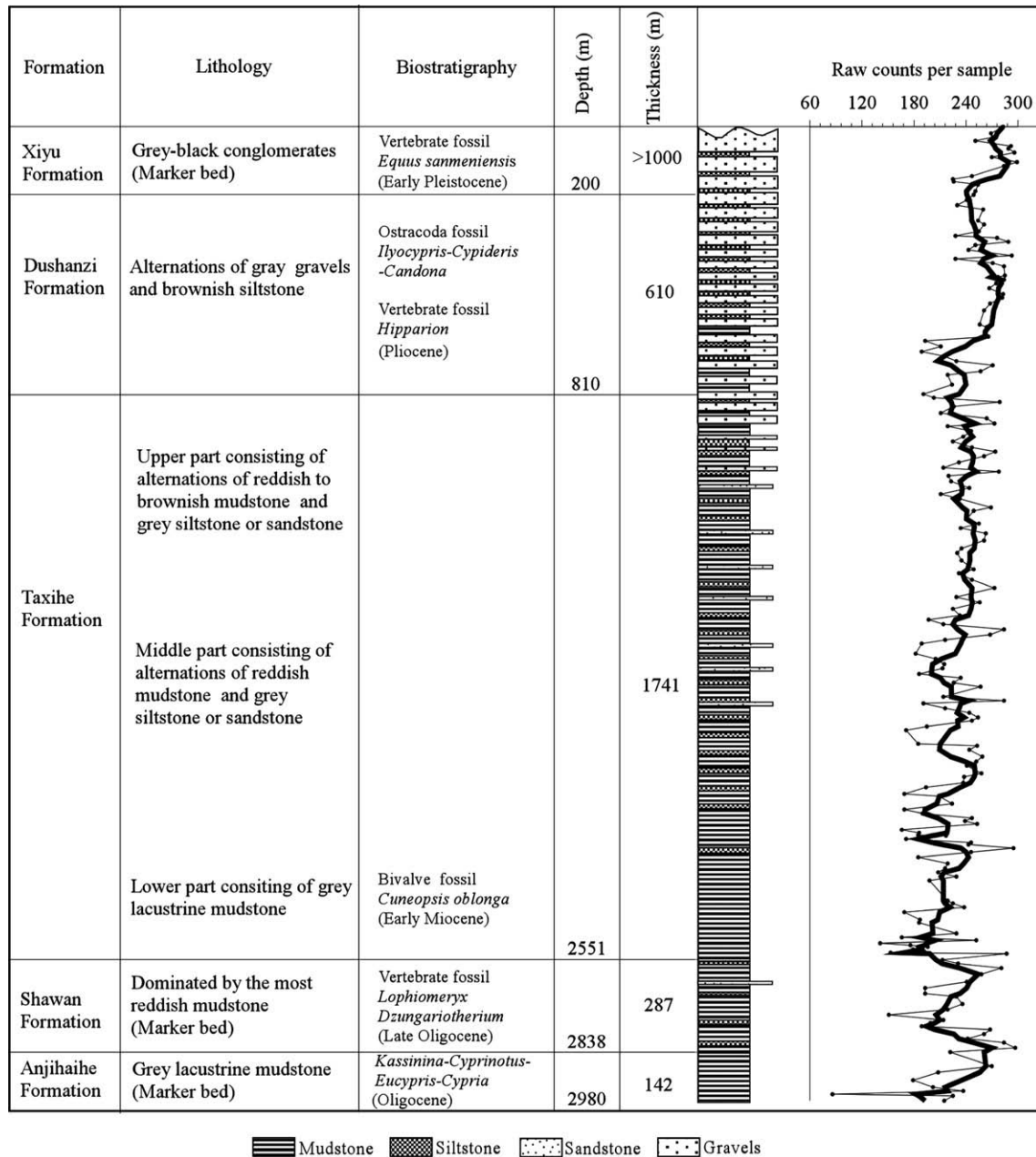
Fig. 4. Lithology, biostratigraphy, and vertical variations in raw pollen counts for each of the analyzed samples. The thick black line in the count data is a 5-point running average. The bivalve fossils in the lower Taxihe Formation were found during the present study; other fossil data are from Chiu (1965, 1973), Peng (1975), Jiang et al. (1995), and Editing Committee of the Stratigraphy of China (1999).
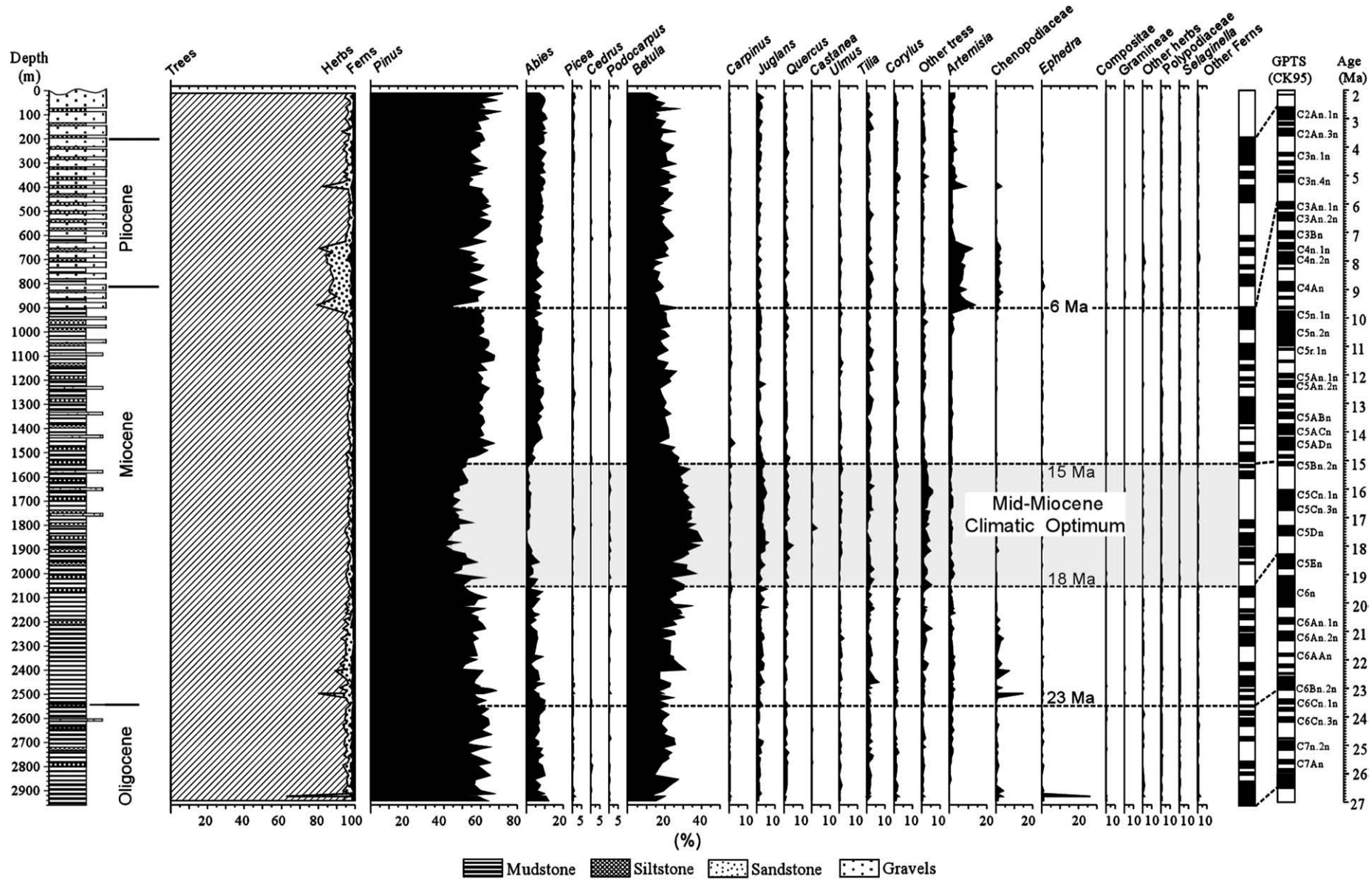
Fig. 5. Pollen diagram showing the percentage abundances of the major floral components within the Taxihe section. Age control is based on biostratigraphic constraints and measured magnetostratigraphy.
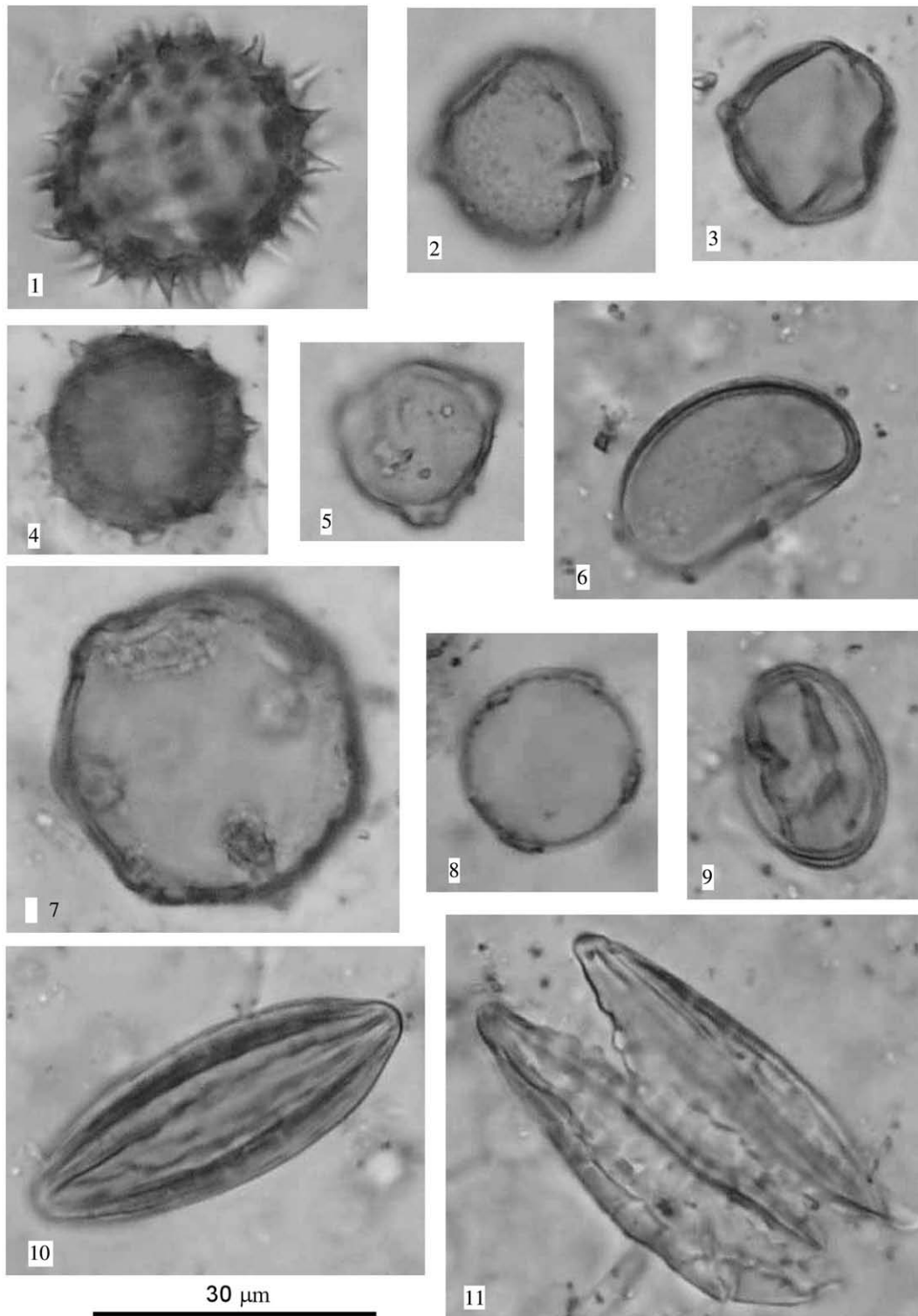
Fig. 6. Representative photographs of pollen grains from the Taxihe section. The slide labels below (e.g., TX05, 11.51) are followed by the England Finder (EF) coordinate. 1, *Aster*, TX05, 11.51, EF K34/4; 2–3, Elaeagnaceae, TX05 11.68, EF F15/3 and M32/2; 4, Compositae, TX05, 21.74, EF O27/4; 5, *Betula*, TX05, 31.67, EF K39/3; 6, Polypodiaceae, TX05, 31.69, EF F26/3; 7, *Juglans*, TX05, 52.37, EF M24/1; 8, *Humulus*, TX05, 61.125, EF L52/3; 9, *Quercus*, TX05, 131.74, EF M25/4; 10–11, *Ephedra*, TX05, 112.38, EF E24/3 and P35/2.

The chronology of Cenozoic terrestrial sedimentary deposits provides the basis for interpreting long-term climate change. For thick piedmont sediments, it is not possible to simply correlate magnetic polarity data with the global polarity time scale (GPTS) of Cande and Kent (1995) without biostratigraphic age control.

In the northern foreland basin of the Tian Shan range, both lithology and biostratigraphy of the studied Taxihe section can be spatially correlated with other sites. The typical thick molasse deposits of the Xiyu Formation (>1000 m thick), the red color of the Shawan Formation, and the characteristic grey lacustrine mudstone of the Anjihaihe Formation all represent marker beds that enable stratigraphic correlation among different sites. The biostratigraphic zones have been defined (Fig. 4), and they are zonations for the region.
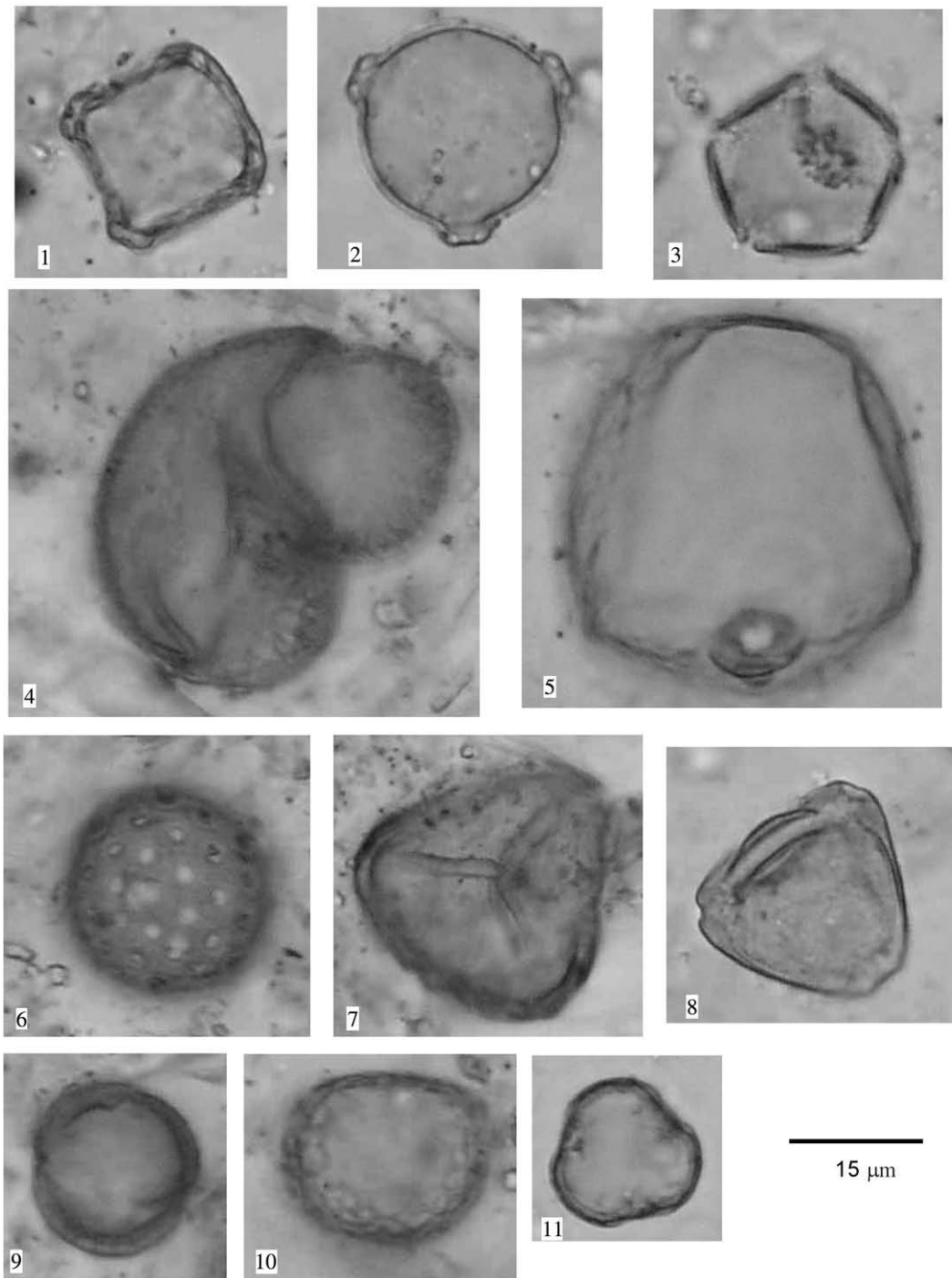
Fig. 7. Representative photographs of pollen grains from the Taxihe section (continued). 1, *Alnus*, TX05, 21.135, EF N36/2; 2, *Carpinus*, TX05, 21.253, EF K34/4; 3, *Pterocarya*, TX05, 31.76, EF M26/3; 4, *Pinus*, TX05, 152.87, EF P39/1; 5, Gramineae, TX05, 37.98, EF L26/3; 6, Chenopodiaceae, TX05, 120.96, EF K26/0; 7, *Selaginella*, TX05, 113.74, EF L28/2; 8, *Corylus*, TX05, 87.39, EF M33/2; 9, *Artemisia*, TX05, 122.28, EF H26/1; 10, *Ulmus*, TX05, 79.63, EF E26/3; 11, Ranunculaceae, TX05, 130.49, EF L38/1.

Fossil of *Uquus sanmeniensis* was found at the base of the uppermost Xiyu Formation in a section close to the present study area (Peng, 1975), suggesting an early Pleistocene age (Fig. 4). Fossils of *Hipparion* in the Dushanzi Formation indicate a Pliocene age (Editing Committee of the Stratigraphy of China (1999). During the present study, we found one zone of *Cuneopsis oblonga*, *Psilunio stoliczkai*, and *Psilunio munieri* bivalve mollusks in the lower part of the Taxihe Formation at a depth of around 2380 m (Fig. 4). In northwestern China, *Cuneopsis oblonga* is thought to indicate an early Miocene age (Xie, 1999). Fossils of *Lophiomeryx* and *Dzungariotherium* have been found

in the middle part of the Shawan Formation in a section close to the present study area (Chiu, 1965, 1973), suggesting a late Oligocene age. Moreover, Jiang et al. (1995) assigned an Oligocene age to an Ostracoda fossil group of *Kassinina–Cyprinotus–Eucypris–Cypria* identified in the Anjihaihe Formation.

Based on the above biostratigraphic age constraints, we compared the measured magnetic polarity sequence of the studied section with the geomagnetic polarity timescale (GPTS) of Cande and Kent (1995) (Sun and Zhang, in press), yielding an age range of 26.5 to 2.6 Ma for the studied section (Fig. 5).

The main characteristics of the pollen diagram shown in Fig. 5 are as follows: (1) the entire section is dominated by tree pollen, of which *Pinus* is the most abundant and the taxa *Betula* and *Abies* are also common; and (2) among the herbs, *Artemisia* and Chenopodiaceae are the most common taxa (Fig. 5). Based on a detailed analysis of trends in the major pollen components, we recognize the following five pollen zones from the studied beds.

4.1. Zone I (2960–2480 m depth, ca. 26.5–23 Ma)

Tree pollen is prominent in Zone I (62.8–97.5%), with *Pinus* being the most abundant (38–68%) (Fig. 5). Other conifer pollens identified are *Abies* (3.6–11.7%) and *Picea* (0–1.2%). Among the deciduous species, *Betula* (13–27%) is prominent, being the second-most abundant species overall; other deciduous species include *Tilia* (0–6.6%), *Juglans* (0–4.2%), and *Quercus* (0–2.7%). Herb taxa make up 1.7–33.7%, dominated by *Ephedra* (0–27%), Chenopodiaceae (0–15%), and *Artemisia* (0–2.6%). Ferns make up 0.7–3.5%.

4.2. Zone II (2480–2050 m depth, ca. 23–18 Ma)

Tree pollen makes up 89.8–97.9%. *Pinus* is the most abundant (50–63%), with the montane conifers *Abies* and *Picea* making up 1.2–8.4% and 0–0.5%, respectively. *Betula* makes up 16–34%, making it the second-most abundant species; other deciduous species include *Tilia* (0.4–6.6%), *Juglans* (0.4–5.4%), and *Quercus* (0–1.9%). The herb taxa make up 0.6–9.1%, dominated by Chenopodiaceae (0–7%) and *Artemisia* (0–3%); ferns represent just 0.5–2.1%. The vegetation type in Zone II is generally similar to that in Zone I, except for a slightly higher proportion of the deciduous species *Juglans* and *Betula*, and lower proportion of the boreal conifer *Abies* (Fig. 5).

4.3. Zone III (2050–1540 m depth, ca. 18–15 Ma)

Tree pollen makes up 94.7–98.1% in Zone III. Although *Pinus* remains abundant (39–62%), Zone III records the lowest *Pinus* percentage of all the zones, as well as the lowest value of the high-altitude conifer *Abies* (0–7%). In contrast, the temperate deciduous species *Betula* (22–41%) and the warm-temperate species *Juglans* (1.5–7%) and *Quercus* (0–5%) show the highest percentages compared with the other pollen zones (Fig. 5). Other minor temperate deciduous species are *Tilia* (0–3.8%), *Ulmus* (0–2.1%), and *Carpinus* (0–1.4%). Herb taxa make up just 1.0–4.1%, dominated by *Artemisia* (0.4–2.6%) and Chenopodiaceae (0–1.5%). Ferns make just a minor contribution (0–2.4%).

4.4. Zone IV (1540–910 m depth, ca. 15–6 Ma)

Tree pollen contributes 90.4–98.6%. *Pinus* (45–68%) is dominant, with the high-altitude conifers *Abies* (2.3–9.1%) and *Picea* (0–1.1%) also making a contribution. *Betula* (16–28%) is the second-most abundant species. Other deciduous species include *Juglans* (0.9–4.7%), *Tilia* (0–3.4%), *Carpinus* (0–3.1%), *Quercus* (0.4–2.8%), and *Ulmus* (0–1.7%). The woody shrub *Corylus* makes up 0.4–2.2%. Herb taxa contribute 0.7–8.7%, dominated by *Artemisia* (0.7–5.5%). Ferns make up just 0–2.4%.

4.5. Zone V (910–0 m depth, ca. 6–2.6 Ma)

Tree pollen contributes 79.5–97.9%. *Pinus* makes up 45–72%, with the high-altitude conifers *Abies* (2.9–11%) and *Picea* (0–1.1%) also making a contribution. The deciduous species include *Betula* (12–26%), *Juglans* (0.4–3.7%), *Tilia* (0–3.6%), *Quercus* (0–2.7%), *Ulmus* (0–1.4%), and *Carpinus* (0–1.3%). The most prominent feature of this zone

is an increase in the contribution of herb taxa (1.4–17.4%), especially *Artemisia* (0.8–14%) and Chenopodiaceae (0–3.6%) (Fig. 5). Ferns make a minor contribution (0–3.7%).

5. Discussion

Pollen records derived from sediments mainly reflect climate change, lithofacies, and tectonic-induced changes in altitude. In the present study, the observed vertical trends in raw pollen counts suggest that the preservation of pollen grains is not significantly affected by lithofacies type (Fig. 4). Moreover, we demonstrate below that changes in altitude had not significant effect on the identified pollen species. Therefore, the pollen record observed in the present study largely reflects the influence of long-term climate change.

5.1. Mid-Miocene Climatic Optimum

The most prominent changes in pollen assemblage recorded in the present study occurred between 18 and 15 Ma (Fig. 5). During this period, the conifer species *Pinus* and *Abies* were less abundant than at other times, whereas the temperate deciduous tree *Betula* and the thermophilous deciduous broadleaved elements of *Juglans* and *Quercus* were more abundant than at other times. The characteristics of the pollen diagram for this period indicate an optimum climate at 18–15 Ma, coincident with the well-known Mid-Miocene Climatic Optimum retrieved from deep-sea deposits, when high-latitude surface-water temperatures were as much as 6 °C warmer than those of today (Savin et al., 1975; Shackleton and Kennett, 1975).

To further aid our paleoclimatic interpretation of the established pollen zones, we performed a principal component analysis of the pollen data. Fig. 8 shows a PCA biplot of pollen percentages. The first principal component, axis 1, accounts for 69.5% of the variance in the pollen spectra; axis 2 accounts for 13.8%. The temperate deciduous species *Betula* has the highest positive loadings on axis 1, whereas the conifer *Pinus* has negative loadings. Compared with the negative loadings of *Pinus*, the positive loadings of *Betula* on axis 1 suggest a warmer and more humid climate. *Artemisia* and *Ephedra* have strong positive loadings on axis 2 (Fig. 8). Because both *Artemisia* and *Ephedra* are herb taxa that grow in arid and semi-arid regions, the positive loadings on axis 2 represent dry climate.

Because the factor scores of the first two principal components account for 83.3% of the variance, we use the scores of the first and second axes of the PCA to describe environmental change represented by the pollen data (Fig. 9). The factor scores on axis 1 clearly show
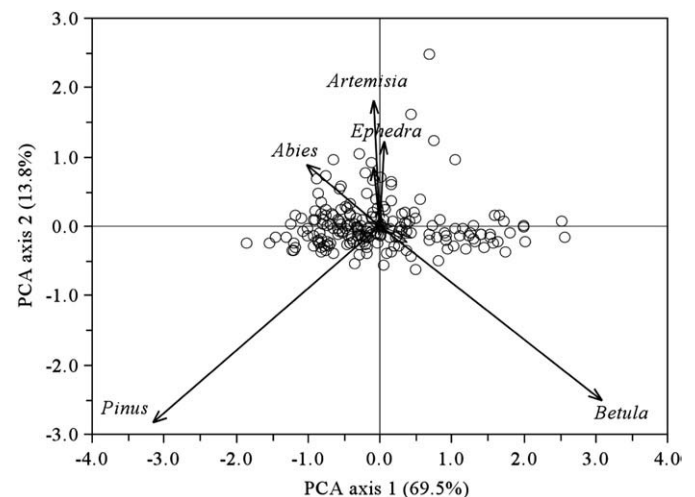

Fig. 8. Principal component analysis (PCA) biplot of pollen species from the Taxihe section. Axes 1 and 2 account for 69.5% and 13.8% of the variance in species abundances, respectively.
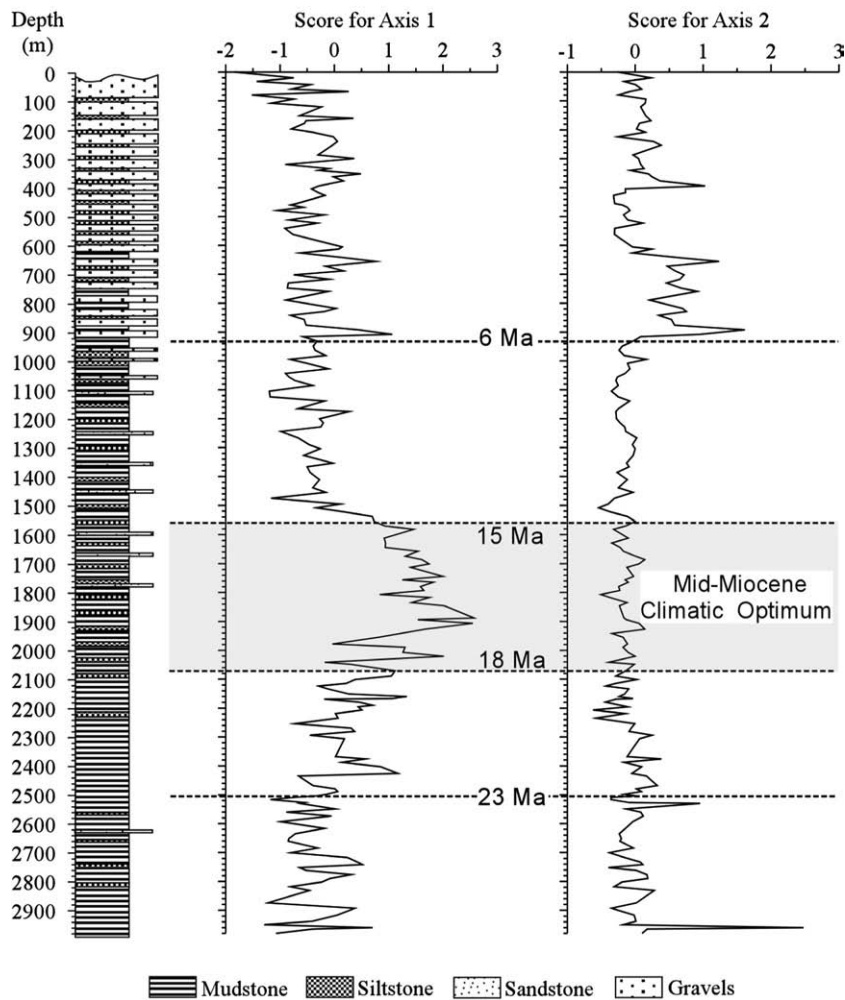
Fig. 9. Vertical variations in the factor scores of PCA axes 1 and 2 throughout the Taxihe section.

higher values at depths of 1560–2070 m, corresponding to an age interval of 15–18 Ma (Fig. 9). As the factor scores on axis 1 suggest a warmer and more humid climate, they indicate an optimum climate at 18–15 Ma. The factor scores on axis 2 indicate high values after 6 Ma. Because axis 2 represents dry climate, the increased scores imply enhanced aridity after 6 Ma.

The Mid-Miocene Climatic Optimum identified from our pollen records can be correlated with similar features identified in pollen records from different areas. For example, White et al. (1997) reported a climatic warm peak at ~15 Ma based on the abundance of thermophilous taxa (including *Fagus* and *Quercus*) in strata from Canada and Alaska, USA. Pollen records also reveal a mid-Miocene subtropical to warm-temperate humid climate in Europe (e.g., Utescher et al., 2000; Jiménez-Morenoa et al., 2005; Jiménez-Moreno and Suc, 2007). Finally, palynological data suggest warm conditions and increased freshwater input at 17–15 Ma in Prydz Bay, East Antarctic (Hannah, 2006).

It is important to emphasize that the marine oxygen isotopic curve of Zachos et al. (2001) shows a remarkable latest Oligocene (24–25 Ma) warming that matches late Eocene temperatures and exceeds those of the Mid-Miocene Climatic Optimum; however, our pollen data do not record this warm event (Figs. 5 and 9). Moreover, the oxygen isotope curve of Miller et al. (1987) also shows only a moderate warming during the latest Oligocene compared with the cold climate of the earliest Oligocene, when the Antarctic ice sheets began to form; the latest Oligocene temperatures did not reach those of the Mid-Miocene Climatic Optimum. Therefore, additional work is

required to determine the extent of climate warming during the latest Oligocene.

5.2. Enhanced aridity since 6 Ma

Another prominent feature of our pollen diagram is an increase in the proportion of herb taxa after ~6 Ma, especially the dominant species *Artemisia* (Fig. 5). Although *Artemisia* first occurred in the study region at ~26 Ma, its abundance was generally less than 2% prior to 6 Ma, whereas it exceeded 14% subsequent to 6 Ma. Modern pollen-rain data obtained from surface samples indicate that *Artemisia* prefers the cooler and more semi-arid environment of northern China (Sun et al., 1996). Therefore, the prominent increase in *Artemisia* recorded after 6 Ma indicates the development of a cool and arid climate in the study region. Pollen data from Central Nepal also suggest climatic cooling at ~6.5–5 Ma, indicated by an increase in the proportion of steppe taxa and a decrease in tropical forest taxa (Hoorn et al., 2000).

It is now known that the ice-rafted detritus (IRD) that settles in the Norwegian Sea can be used to monitor the flux of icebergs derived from glaciers and ice sheets in the high latitudes of the Northern Hemisphere (e.g., Jansen and Sjøholm, 1991; Wolf and Thiede, 1991). Based on IRD records since ~5.5 Ma, Jansen and Sjøholm (1991) suggested that the glaciers or ice sheets must have been large enough to reach sea level at high latitudes in the Northern Hemisphere. Climate records in both west Antarctica (Kennett and Barker, 1990) and the Arctic (Thiede and Vorren, 1994) also indicate cooling and ice-

sheet expansion since 6 Ma. In a similar vein, stable carbon isotopic studies of fossil soils from Pakistan and North America reveal the expansion of C_4 grasses at 8–6 Ma, thereby indicating the development of an arid climate since the latest Miocene (Cerling et al., 1993, 1997). Therefore, the cool and dry climate inferred from our pollen records for the period after 6 Ma is consistent with interpretations made from other climate records in different parts of the world. These interpretations are supported by our PCA results, which indicate enhanced aridity after 6 Ma (Fig. 9).

5.3. Tectonic uplift vs. climate as a determinant of the pollen record considered in the present study

Given that the studied section is located in an active tectonic region, it is important to consider the influence on vegetation type of temporal changes in altitude (especially for the high-altitude species *Abies* and *Picea*).

The Tian Shan Range was uplifted during the late Paleozoic (Windley et al., 1990), eroded during most of the Mesozoic and early Cenozoic, and reactivated during the late Cenozoic in response to intracontinental deformation within the India–Eurasia collision system. Late Cenozoic uplift began at around 7 Ma (Sun et al., 2004). Within the Taxihe section considered in the present study, the proximal coarse molasse deposits began to accumulate at around 6 Ma, related to mountain uplift and rock denudation and transportation processes (Fig. 5). Deposits prior to 6 Ma are dominated by distal fine lacustrine sediments, they are not evidence of tectonic uplift. Therefore, the Mid-Miocene Climatic Optimum identified from the pollen record is not related to tectonic factors. Although the uplift in the study region occurred after 7–6 Ma, our pollen record shows no remarkable increase in abundance of the high-altitude species *Abies* and *Picea* after 6 Ma, suggesting that tectonic uplift was not a significant controlling factor on pollen assemblage. We did, however, observe an increase in the abundance of the arid species *Artemisia* and Chenopodiaceae after 6 Ma, possibly reflecting the uplift of mountain ranges that acted as a barrier to the influence of the Indian and/or Atlantic Oceans on the climate of the continental interior. However, the initiation of glaciation in the Northern Hemisphere also occurred at ~7– 6 Ma ago (Larsen et al., 1994), meaning that the enhanced aridity indicated by our pollen records after 6 Ma is largely a response to late Cenozoic climatic deterioration.

6. Conclusion

Based on a palynological analysis of late Cenozoic deposits in the northern foreland basin of the Tian Shan Range, we reconstructed vegetation and climate change between 26.5 and 2.6 Ma.

The conifer species *Pinus* and the temperate deciduous tree *Betula* were the most abundant species in this region over the study period. The most remarkable feature of our pollen diagram occurred at 18– 15 Ma, which was marked by the lowest recorded abundances of the conifer species *Pinus* and *Abies*, and the highest abundances of *Betula* and the thermophilous broadleaved trees *Juglans* and *Quercus*. These trends enable the identification of the Mid-Miocene Climatic Optimum in the study region.

Another notable change occurred at ~6 Ma, characterized by an increase in the abundance of herb taxa, especially the steppe to dry steppe taxa *Artemisia* and Chenopodiaceae. These trends suggest a cooler and drier climate since 6 Ma, being mostly a response to late Cenozoic climatic deterioration in the Northern Hemisphere; tectonic uplift of the Tian Shan Range may also have made a minor contribution to these trends.

References

Allen, M.B., Windley, B.F., Zhang, C., 1992. Palaeozoic collisional tectonics and magmatism of the Chinese Tien Shan, Central Asian. Tectonophysics 220, 89–115.
Avouac, J.P., Tapponnier, P., Bai, M., Hou, Y., Wang, G., 1993. Active thrusting and folding along the northeastern Tienshan, and rotation of Tarim relative to Dzungaria and Kazakhstan. Journal of Geophysical Research 98, 6755–6804.
Burchfiel, B.C., Brown, E.T., Deng, Q.D., Feng, X.Y., Li, J., Molnar, P., Shi, J.B., Wu, Z.M., You, H.C., 1999. Crustal shortening on the margins of the Tien Shan, Xinjiang, China. Intertional Geology Reviews 41, 665–700.
Cande, S.C., Kent, D.V., 1995. Revised calibration of the geomagnetic polarity timescale for the Late Cretaceous and Cenozoic. Journal of Geophysical Research 100, 6093–6095.
Cerling, T.E., Wang, Y., Quade, J., 1993. Expansion of C4 ecosystems as an indicator of global ecological change in the Miocene. Nature 361, 344–345.
Cerling, T.E., Harris, J.M., MacFadden, B.J., Leakey, M.G., Quade, J., Eisenmann, V., Ehleringer, J.R., 1997. Global vegetation change through the Miocene/Pliocene boundary. Nature 389, 153–158.
Chiu, C.S., 1965. New findings of Lophiomeryx in China. Vertebrata PalAsiatica 9, 395–398.
Chiu, C.S., 1973. A new genus of giant rhinoceros from Oligocene of Dzungaria, Sinkiang. Vertebrata PalAsiatica 11, 182–191.
Deng, Q.D., Feng, X.Y., Zhang, P.Z., Xu, X.W., Yang, X.P., Peng, S.Z., Li, J., 2000. Active Tectonics of the Tianshan Mountains. Seismology Press, Beijing.
Editing Committee of the Stratigraphy of China, 1999. Stratigraphy in China (Tertiary). Geology Press, Beijing.
Escutia, C., De Santis, L., Donda, F., Dunbar, R.B., Cooper, A.K., Brancolini, G., Eittreim, S.L., 2005. Cenozoic ice sheet history from East Antarctic Wilkes Land continental margin sediments. Global and Planetary Change 45, 51–81.
Faegri, K., Iversen, J., 1989. Textbook of Pollen Analysis. Wiley, New York.
Flower, B.P., Kennett, J.P., 1994. The middle Miocene climatic transition: East Antarctic ice sheet development, deep ocean circulation and global carbon cycling. Paleogeography, Paleoclimatolology, Paleoecology 108, 537–555.
Fu, B.H., Lin, A.M., Kano, K., Maruyama, T., Guo, J.M., 2003. Quaternary folding of the eastern Tianshan, Northwest China. Tectonophysics 369, 79–101.
Gao, J., Li, M.S., Xiao, X.C., Tang, Y.Q., He, G.Q., 1998. Paleozoic tectonic evolution of the Tianshan Orogen, northwestern China. Tectonophysics 287, 213–231.
Hannah, M.J., 2006. The palynology of ODP site 1165, Prydz Bay, East Antarctica: a record of Miocene glacial advance and retreat. Palaeogeography, Palaeoclimatology, Palaeoecology 231, 120–133.
Hendrix, M.S., Dumitru, T.A., Graham, S.A., 1994. Late Oligocene–early Miocene unroofing in the Chinese Tian Shan: an early effect of the India–Asia collision. Geology 22, 487–490.
Hoorn, C., Ohja, T., Quade, J., 2000. Palynological evidence for vegetation development and climatic change in the Sub-Himalayan Zone (Neogene, Central Nepal). Palaeogeography, Palaeoclimatology, Palaeoecology 163, 133–161.
Hu, Z.H., Sarjeant, W.A.S., 1992. Cenozoic spore-pollen assemblage zones from the shelf of the East China Sea. Review of Palaeobotany and Palynology 72, 103–118.
Jansen, E., Sjøholm, J., 1991. Reconstruction of glaciation over the past 6 million years from ice-borne deposits in the Norwegian Sea. Nature 349, 600–604.
Jiang, X., Zhou, Y., Lin, S., 1995. Strata and Ostracoda Fossils in Xinjiang. Geology Press, Beijing.
Jiménez-Moreno, G., Suc, J.P., 2007. Middle Miocene latitudinal climatic gradient in Western Europe: evidence from pollen records. Palaeogeography, Palaeoclimatology, Palaeoecology 253, 208–225.
Jiménez-Morenoa, G., Rodríguez-Tovara, F.J., Pardo-Igúzquizac, U., Fauquetted, S., Suc, J.P., Müller, P., 2005. High-resolution palynological analysis in late early–middle Miocene core from the Pannonian Basin, Hungary: climatic changes, astronomical forcing and eustatic fluctuations in the Central Paratethys. Palaeogeography, Palaeoclimatology, Palaeoecology 216, 73–97.
Kennett, J.P., Barker, P.F., 1990. Latest Cretaceous to Cenozoic climate and oceanographic developments in the Weddell Sea, Antarctica: an ocean-drilling perspective. Proceedings of the Ocean Drilling Program, Scientific Results 113, 937–962.
Larsen, H.C., Saunders, A.D., Clift, P.D., Beget, J., Wei, W., Spezzaferri, S., ODP Leg 152 Scientific Party, 1994. Seven million years of glaciation in Greenland. Science 13, 952–955.
Liang, M.M., Bruch, A., Collinson, M., Mosbrugger, V., Li, C.S., Sun, Q.G., Hilton, J., 2003. Testing the climatic estimates from different palaeobotanical methods: an example from the Middle Miocene Shanwang flora of China. Palaeogeography, Palaeoclimatology, Palaeoecology 198, 279–301.
Liu, G.W., Leopold, E.B., 1994. Climatic comparison of Miocene pollen floras from northern East-China and south-central Alaska. Paleogeography, Paleoclimatology and Paleobotany 108, 217–228.
Ma, Y., Li, J., Fan, X., 1998. Pollen-based vegetational and climatic records during 30.6 to 5.0 My from Linxia area, Gansu. Chinese Science Bulletins 43, 301–304 (in Chinese).

Ma, Y., Fang, X., Li, J., Wu, F., Zhang, J., 2004. Vegetational and environmental changes during late Tertiary–early Quaternary in Jiuxi Basin. Science in China (Series D) 34, 107–116 (in Chinese).

Miller, K.G., Fairbanks, R.G., Mountain, G.S., 1987. Tertiary oxygen isotope synthesis, sea level history, and continental margin erosion. Paleoceanography 2, 1–19.

Peng, X.L., 1975. Positions and stratigraphical control of the Cenozoic mammalian fossils in the Junggar Basin of Xinjiang. Vertebrata PalAsiatica 13, 185–189.

Savin, S.M., Douglas, R.G., Stehli, F.G., 1975. Tertiary marine paleotemperatures. Geological Society of America Bulletin 86, 1499–1510.

Shackleton, N.J., Kennett, J.P., 1975. Paleotemperature history of the Cenozoic and the initiation of Antarctic glaciation: oxygen and carbon isotopic analyses in DSDP Sites 277, 279, and 281. Initial Reports of the Deep Sea Drilling Project 29, 743–755.

Sun, J.M., Zhang, Z.Q., in press. Syntectonic Growth Strata and Implications for Late Cenozoic Tectonic Uplift in the Middle Part of the Tian Shan Range. Tectonophysics.

Sun, J.M., Zhu, R.X., Bowler, J., 2004. Timing of the Tianshan Mountains uplift constrained by magnetostratigraphic analysis of molasse deposits. Earth and Planetary Science Letters 219, 239–253.

Sun, J.M., Xu, Q.H., Huang, B.C., 2007. Late Cenozoic magnetochronology and paleoenvironmental changes in the northern foreland basin of the Tian Shan Mountains. Journal of Geophysical Research 112. doi:10.1029/2006JB004653.

Sun, X.J., Song, C., Wang, F., 1996. Pollen-climate response surface of selected taxa from northern China. Science in China (Series D) 39, 486–493.

Sun, X.J., Wang, P.X., 2005. How old is the Asia monsoon system? — palaeobotanical records from China. Palaeogeography Palaeoclimatology Palaeoecology 222, 181–222.

Thiede, J., Vorren, T.O., 1994. The Arctic Ocean and its geologic record: research history and perspectives. Marine Geology 119, 179–184.

Utescher, T., Mosbrugger, V., Ashraf, A., 2000. Terrestrial climate evolution in Northwest Germany over the last 25 million years. Palaios 15, 430–449.

Wang, W.M., 1990. Sporo-pollen assemblages from the Miocene Tonggure formation of Inner Mongolia and its climate. Acta Botanica Sinica 32, 901–904.

Wang, D.N., Sun, X.Y., Zhao, Y.N., 1990. Late Cretaceous to Tertiary palynofloras in Xinjiang and Qinghai, China. Review of Palaeobotany and Palynology 65, 95–104.

White, J.M., Ager, T.A., Adam, D.P., Leopold, E.B., Liu, G., Jetté, H., Schweger, C.E., 1997. An 18 million year record of vegetation and climate change in northwestern Canada and Alaska: tectonic and global climatic correlates. Palaeogeography, Palaeoclimatology, Palaeoecology 130, 293–306.

Windley, B.F., Allen, M.B., Zhang, C., Zhao, Z.Y., Wang, G.R., 1990. Paleozoic accretion and Cenozoic redeformation of the Chinese Tianshan Range, central Asia. Geology 18, 128–131.

Wolf, T.C.W., Thiede, J., 1991. History of terrigenous sedimentation during the past 10 My in the North Atlantic (ODP Legs 104 and105 and DSDP Leg). Marine Geology 101, 83–102.

Xie, G.P., 1999. Tertiary bivalves from the Xianshuihe Formation of Lanzhou Basin, Gansu. Acta Palaeontologica Sinica, 38, 94–101.

Xu, J.X., Ferguson, D.K., Li, C.S., Wang, Y.F., 2008. Late Miocene vegetation and climate of the Lühe region in Yunnan, southwestern China. Review of Palaeobotany and Palynology 148, 36–59.

Yin, A., Nie, S., Craig, P., Harrison, T.M., Ryerson, F.J., Qian, X., Yang, G., 1998. Late Cenozoic Tectonic evolution of the southern Chinese Tian Shan. Tectonics 17, 1–27.

Zachos, J., Pagani, M., Sloan, L., Thomas, E., Billups, K., 2001. Trends, rhythms, and aberrations in global climate: 65 Ma to present. Science 292, 686–693.